Tribological behavior of firm kaolin against smooth rigid wall during extrusion process

Viet Hai Hoang, Christophe Lanos, Yannick Mélinge

Applications in Engineering Science 17 (2024) 100175

Contents lists available at ScienceDirect

Applications in Engineering Science

journal homepage: www.sciencedirect.com/journal/applications-in-engineering-science

Tribological behavior of firm kaolin against smooth rigid wall during extrusion process

Viet Hai Hoang [a,*], Christophe Lanos [b], Yannick Mélinge [c]

[a] Faculty of Civil Engineering, University of Transport and Communications, 3 Cau Giay, Lang Thuong, Dong Da, Hanoi, Vietnam
[b] Laboratoire de Génie Civil et Génie Mécanique, UNIR, Université de Rennes, 3 rue du Clos Courtel, Rennes 35704, France
[c] Laboratoire de Recherche des Monuments Historiques (LRMH – CRC UAR 3224 CNRS), 29 Rue de Paris, Champs sur Marne 77420, France

ARTICLE INFO

Keywords:
Tribological behavior
Extrudable kaolin
Tribometer

ABSTRACT

One of the main factors influencing the quality of production shape and energy consumption in an extrusion process is the interaction between the material and the wall. To investigate the tribological behavior of extrudable kaolin and a rigid wall, a tribometer is specifically designed and validated for measuring friction at the kaolin-wall interface. Compared to another tribometer in the literature, this device permits the variation of the normal stresses at the wall/material interface during testing. Finally, the tribological behavior of kaolin friction is determined within a range of velocities from $10^{-}3$ m/s to 5.10^{-2} m/s and a range of normal stress from 120 to 250 kPa.

1. Introduction

Extrusion is a widely used forming industrial process in various fields such as food, polymer, clay, metal (Ulrich and Binz, 2021; Jayasimha et al., 2022) and cement paste (Akhoundi and Ouzah, 2023; Akhoundi and Sousani, 2023; Perrot et al., 2019). The advantages of this technique enable high productivity and improvement in the mechanical properties of the formed product. One of the main factors influencing extrusion capacity and the quality of product shape is the friction between the walls of the extrusion device and the extrudable materials, as shown in Fig. 1. Friction may not only occur in the die system area (Benbow and Bridgewater, 1993), but also appear at the interface between the extruder barrel and forming material, as indicated in several research studies (Perrot et al., 2006). Friction force depends on the surface finish of the wall (Nguyen, 2022; Nguyen et al., 2022; Tran et al., 2022) the normal load applied to the extrudable material at the interface, as shown in Fig. 1.

To gain a better understanding of the flow properties of extrudable materials during the extrusion process and to improve flow modeling (Perrot et al.), it is necessary to study the friction behavior between a metal wall and material using a dedicated device called a 'tribometer.' Due to the significant evolution of radial normal stress in inside the extruder barrel and the assumption of plug flow along the extruder barrel (Fig. 1), a linear configuration can be employed for the tribological investigation instead of a cylindrical configuration. To better simulate the tribological behavior in the extrusion process, the development of the tribometer needs to take into account the following factors: the effect of local stress variations, the effect of slipping velocity, the effect of wall roughness, and a sufficiently long or infinite friction path.

Perrot et al. (2006, 2012) used a ram extruder to study the tribological behavior of high yield stress fluids during the extrusion process by measuring the evolution of total extrusion force versus the billet length. However, this device cannot directly measure the friction force and radial force applied to the material at the interface. Some studies in the literature have focused on reducing friction force. Hoang et al. (2023) employed electro-osmosis to decrease the friction force between cement paste-based material and a metal wall, while Goudjil et al. (2012), Vanhove and Djelal (2021) utilized this process in formwork removal.

The choice of tribometer configuration in this research is based on an analysis of several types of tribometers used to study friction at the steel/material interface. The first type of tribometer is employed to identify friction at the steel-concrete interface under pumping conditions (Kandagaddala et al., 2023; Ngo et al., 2010). Using a modified Couette geometry, it can determine interface friction, layer material composition, and can be used on construction sites due to its mobility and efficient testing procedure. However, this tribometer cannot account for the high

* Corresponding author.
E-mail address: hoangviethai@utc.edu.vn (V.H. Hoang).

https://doi.org/10.1016/j.apples.2024.100175
Received 10 January 2024; Accepted 21 January 2024
Available online 24 January 2024

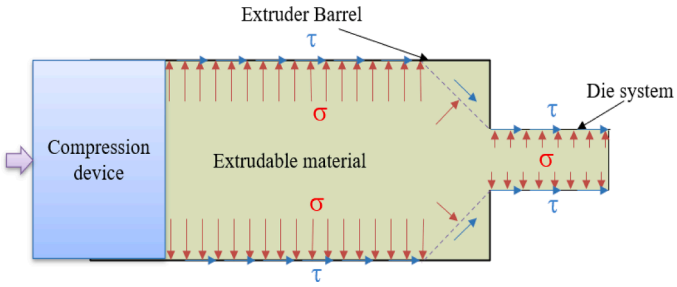

Fig. 1. Schematic of ram extrusion and evolution of stresses during extrusion process.

stress levels applying to materials during extrusion processes. The second type of tribometer (plan/plan tribometer with rectilinear motion) was developed by Djelal (2001), Kocserha and Gömze (2010), Libessart et al. (2020), Spitz et al. (2021) and Vanhove and Djelal (2021). This device operates by applying a constant force to press fresh concrete/paste clay specimens against a moving metal surface, allowing measurement of the tangential force to determine friction between fresh concrete and the metal surface. However, the device cannot locally modify the force acting on the specimen during tribological testing. The third type of tribometer is a modified pawn-on-disc tribometer, designed and validated by Hoang (2011) and Mélinge et al. (2013), which is used to study dynamic friction between a solid body in motion and the cement paste. Another device was used to study the tribology of clay paste (Vignes et al., 2013; Xia et al., 2022), but it is not suitable for describing the stress state of the material during extrusion process.

In this study, a novel tribometer has been developed, enabling the investigation of the tribological behavior of high yield stress fluids (with a shear yield stress larger than 1 kPa) (Perrot et al., 2012). The developed apparatus is capable of measuring the friction force between the material and a smooth wall. The performance of tribometer is discussed, including the calibration procedure, and a data analysis method is proposed at the end of this section. Finally, this tribometer is tested with a kaolin clay paste to examine the tribological behavior, considering the increased normal load and the velocity movement of the wall.

2. Experimental devices and test protocols

2.1. Pawn-on-disc tribometer

A global view of a tribometer is shown in Fig. 2. This device comprises three principal parts: a force measurement device, a rotating plate, and a frame including two motors. The principal operation of this tribometer is the same as that of the pawn-on-disc tribometer used in metallurgy. The smooth wall is composed of a rotating disc with a diameter more than 10 times larger than that of the specimen.

The force measurement device is equipped with four force sensors (ETRAN sensors & Electronics ELFS-T4M*-500-/C2) capable of measuring traction-compression forces within a load range of ± 500 N. The schematic arrangement of these sensors is shown in Fig. 2c. One sensor is dedicated to measuring the vertical force, while the remaining three are used to capture the horizontal forces. The force measurement cell is made from an aluminum alloy block (AU4G) as shown in Fig. 3, and a sample holder made of stainless steel. This choice of materials aims to limit chemical interactions between the material and the sample holder.

The rotating plate compose of a steel disc with a diameter of 40 cm and a thickness of 20 mm. The friction path is created using an annulus made of stainless steel, with a width of 50 mm and a thickness of 8 mm. The maximum diameter of the annulus is 400 mm, and it is screwed onto the plate. The ratio between the specimen diameter (35 mm) and the plate radius (175 mm) (this radius is the distance from the plate center to the sample holder center): $d/R = 0.2$ is small, and the curvilinear

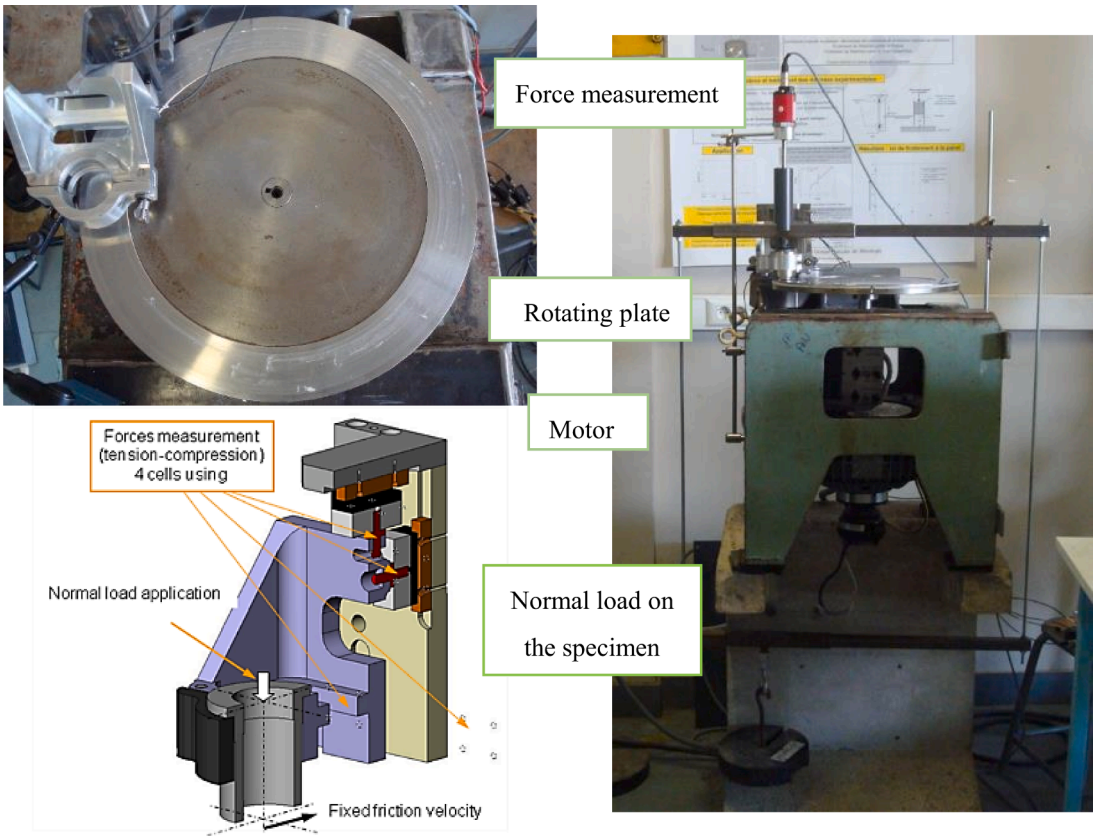

Fig. 2. (a) global view of tribometer; (b) Plan views of tribometer; (c) detail of the force measurement device.

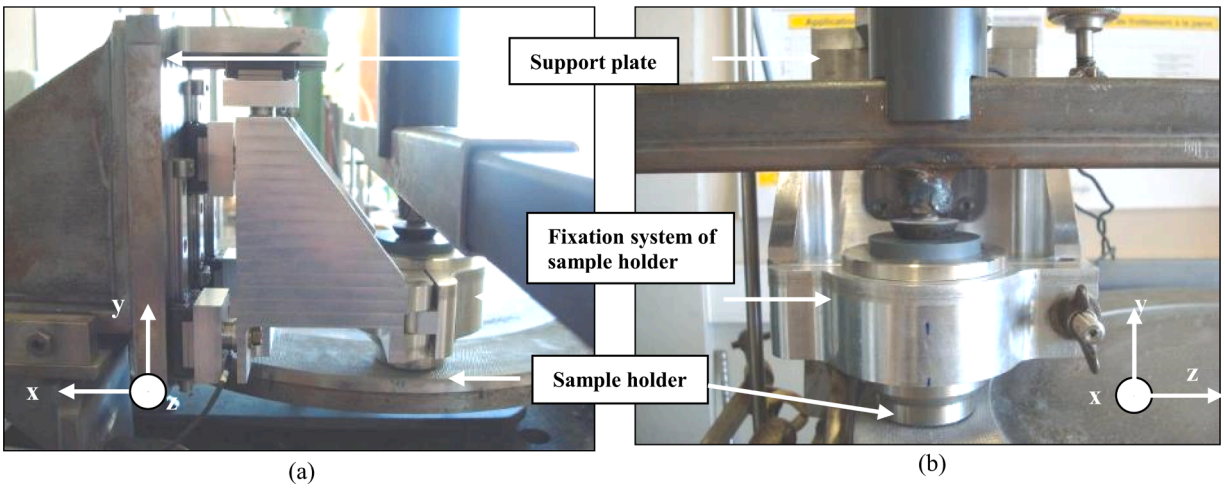

Fig. 3. View of force measurement cell and sample holder: (a) in the plane (x,y); (b) in the plane (y,z).

character induced by the circular geometry of the plate can be neglected.

The plate is rotated and kept at a constant velocity through the combined action of two motors. This association is capable of covering a velocity range of the rotating plate from 0 to 3000 tr/min: Engine DC motor, series M, CEM Company Electro Meca, noted motor 1; Engine DC motor, series M, CEM Company Electro Meca, noted motor 2. Two motors are connected to the power circuit and an individual potentiometric system that allows rotation velocity modulation of each motor. These motors can operate alone or together, covering a wide range of velocity and maintaining the maximum torque value from one to two motors. Due to the power of two motors, the tribometer can operate with an imposed constant velocity regardless of the imposed load.

The voltages supplied by sensors 1, 3, 4, and 5, as well as the tachometer probe, are captured and recorded using an acquisition system (SI3535F Schlumberger) (see Figs. 8 and 9). The recorded data are processed using Lookout FMS software, which features a graphical user interface and dialogues.

To accurately determine the influence of the normal force at the interface between the specimen and plate, it is necessary to measure the forces resulting from the interaction between the specimen and its holder. This can be achieved by intentionally misaligning the axes of the plate and motor shaft (Fig 5a), causing a vertical oscillation disturbance in the plate. The purpose of this disturbance is to create a measurable interaction between the specimen and sample holder, facilitating the characterization of dissipation energy at the specimen/plate interface.

The vertical position of the contact surface between the specimen and the plateau during the rotating of plate is measured in the laboratory Cartesian coordinate system (G; x, y, z) (Fig. 5) as a function of the rotation angle α. Then, the evolution of this position as shown in Fig. 4b can be modeled by a sinusoidal function as equation following:

$$\Delta y(\alpha) = y_0 + \frac{A_{\max}}{2}\cdot\sin(\alpha + \phi) \quad (1)$$

Where: A_{max} is the maximal amplitude; y_0 et φ are constants.

Knowing plate rotation velocity allows us to evaluate oscillation rate and acceleration imposed by plate on the specimen.

2.2. Mechanical study of system

Fig. 5 illustrates the relationship between horizontal and vertical forces at the material/plate interface (with its application point located at point R) and the forces measured at points A_1, A_2, A_3, and C. This crucial step is conducted prior to the manufacture of the tribometer and during the tribometer design phase, aiming to minimize unavoidable errors in the measurement procedure.

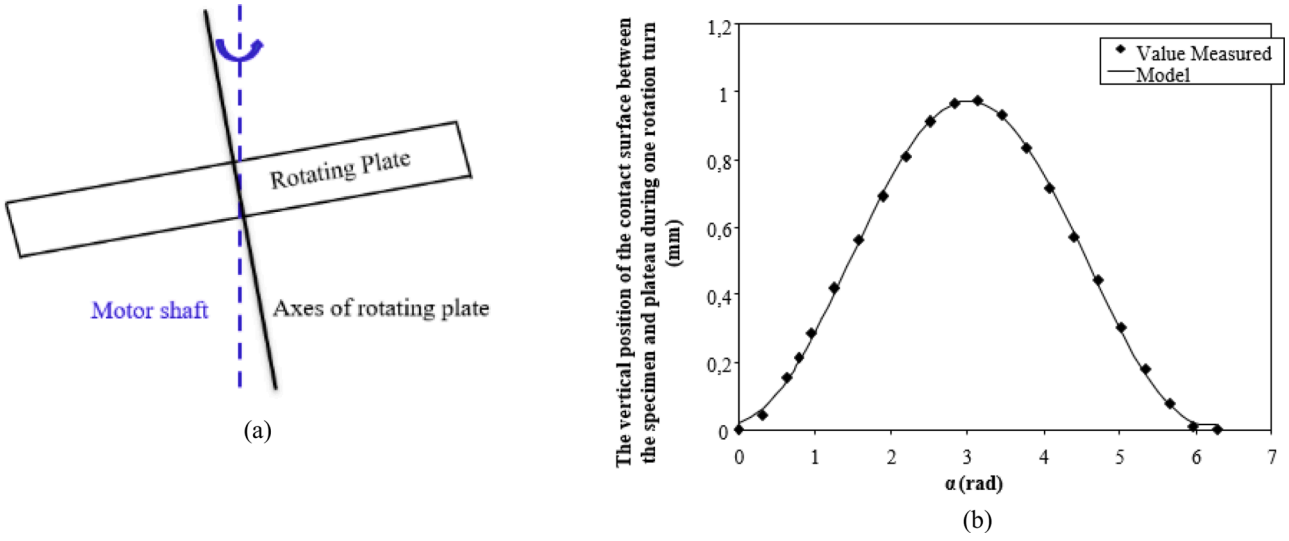

Fig. 4. (a) The misaligning the axes of the plate and motor shaft; (b) The vertical position of the contact surface between the specimen and plateau during one rotation turn.

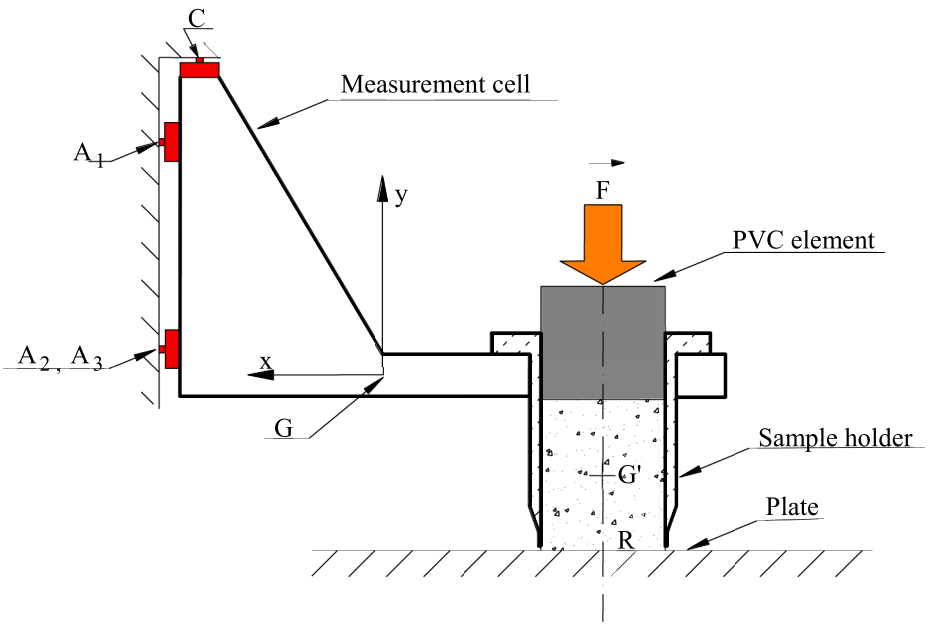

Fig. 5. Schematic of calculation of horizontal and vertical forces at interface material/rotating plate; where G is the center of gravity of the measurement cell, G' is the center of gravity of the specimen and R is this of the contact surface between the specimen and the rotating plate.

The investigation of the mechanical aspects of the system, within the domain of particle mechanics, involves the introduction of a mechanical equation and is carried out in two consecutive steps. Firstly, we examine the equilibrium of the measurement cell by utilizing general theorems. This includes balancing the equations and simplifying them at the center of gravity of the measurement cell (point G). This initial study enables the identification of a mechanical equation at point B, representing the center of gravity of the contact surface between the specimen and the sample holder. Secondly, the equilibrium of specimen is analyzed, establishing a relationship between the equation at the center of gravity of the specimen/rotating plate interface (point R) and the equation at point B. By combining these two steps, the balance equation and the relationship between pairs of forces (Rx, Ry) and (Bx, By) are established, as well as the forces measured at points A_1, A_2, A_3, and C, as shown in Eqs. (2) and (3).

$$\begin{cases} -B_x + R_x = m\dfrac{dV_x}{d_t} \\ -B_y + R_y + F_y + P_y = m\dfrac{dV_y}{d_t} \end{cases} \tag{2}$$

$$\begin{cases} B_x + A_{1x} + A_{2x} + A_{3x} = 0 \\ B_y + C_y = 0 \end{cases} \tag{3}$$

Where: V_x and V_y are the velocity of the specimen in the direction x and in the direction y, respectively

2.3. Calibration

The calibration of a tribometer was conducted in two cases: static calibration, which establishes a histogram of data treatment, and dynamic calibration, which verifies the appropriate application of laws established in the static case to the dynamic case.

(a) *Static calibration and histogram calculation*

The principle of static calibration involves applying forcing loads to the force measurement cell and observing the response of the tribometer. To simulate a real test, the application point and load range remain exactly the same during a tribological characterization test.

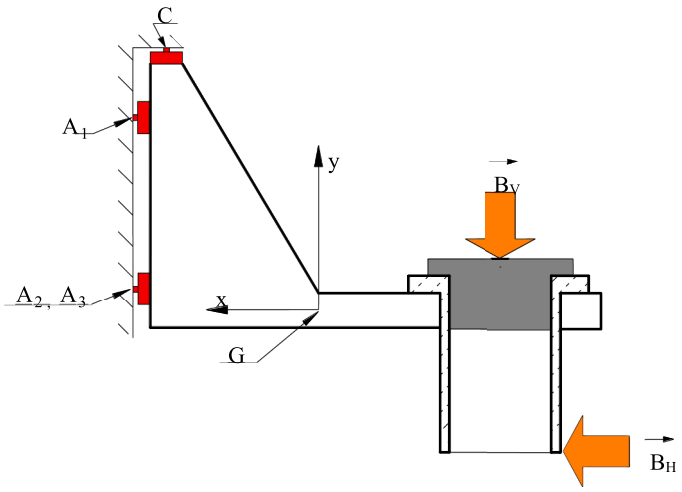

Fig. 6. Schematic of calibration static.

Fig. 6 presents a schematic of the calibration test.

To distinguish the effects of vertical and horizontal loads on recorded data and establish the relationship between these two variables, two test series are conducted. In the first series, only standard masses are vertically placed on the sample holder ($B_H = 0$). In the second series, a combination of vertical and horizontal loads is applied. The tests are conducted by maintaining a constant vertical load (B_y) as in the first series while incrementing the horizontal load (B_H). The selected load values are compatible with the measured force in the tribometer test.

(a) *Dynamic calibration*

Dynamic calibration is performed using a texture analyzer distributed by Stable Micro Systems. Fig. 7 shows a schematic view of this machine and illustrates its assembly with the force measurement device of the tribometer.

The Texture Analyzer operates with imposed displacement. Two amplitudes are used: 0.1 and 0.2 mm, with a frequency $f = 0.1$ Hz. Figs. 8 and 9 show the temporal evolution of the force applied by the Texture

Fig. 7. Testing the response of the measurement cell with the Texture Analyzer.

Analyzer and the measured forces at the measurement cell using a static calibration law. Both amplitude conditions of the sinusoidal signal have demonstrated a good reproduction of information in two cases: vertical positioning and horizontal positioning of the measurement cell.

3. Friction discussion and model

3.1. Material and test

The used material is a mixture of kaolin clay powder and water, with a water/kaolin mass ratio of 35 %. The kaolin is sourced from the quarries at Ploemeur (Morbihan) (Polwhite BB). Fig. 10 shows the mineralogical content of this material determining by X-ray diffraction. The X-ray diffraction analysis indicated the predominant presence of kaolinite (denoted as K in Fig. 10) and, to a lesser extent, illite (denoted as I in Fig. 10).

The liquid and plasticity limits of this material were determined equal to 55 % and 39 %, respectively. This material is composed of kaolin clay (0–10 μm, with the largest clay grain size close to 4 μm).

The kaolin powder was initially mixed with a water content of 35 %. This mixture was then passed through a screw extruder with die extruder ($d = 35$ mm) to ensure pre-compaction and homogenization of mixture. The extrudates were kept moist in a sealed bag to maintain humidification and were used for tribological characterization in a tribometer.

A Brookfield tester was utilized to determine the rheological behavior of kaolin pastes. This device is equipped with a vane geometry, where the diameter and height of the four-bladed vane are 10 mm each. Tests were conducted at a constant rotation rate of 0.01 rad s^{-1}, as demonstrated in a previous study (Liddel and Boger, 1996). This protocol allows for the determination of the yield stress, with negligible consideration for viscous effects. The kaolin paste exhibits a visco-plastic behavior, manifesting a yield stress of approximately 45 ± 4 kPa.

4. Test protocol

The tests are conducted in two steps. Initially, after placing the extrudate of kaolin with the initial height ($H = 40$ mm) on the sample holder, the specimen is pre-consolidated under a constant load. This load value is subsequently employed in friction test protocol. The introduction of the first step in the protocol aims to prevent specimen compaction during the friction test. As shown in Fig. 11a, the duration that the height reached constant is about 240 min for a vertical load with a range from 120 to 250 kPa.

4.1. Structuration of specimen

When keeping the vertical load on the top of the specimen, the setting curve of specimen during times was recorded until the height of specimen stabilizes. Consequently, once the height stabilization is achieved (after 240 min).

4.2. Tribological behavior of firm kaolin at low velocity

The tangential stress curves versus normal stress at the kaolin/smooth wall (Ra = 0.52 μm) interface for two tests at low friction velocity ($V_g = 10^{-3}$ m/s) are depicted in Fig. 12. The experimental data are recorded for only half a plate rotation, corresponding to the structuration phase of kaolin paste. Two distinct tests (with two distinct loadings)

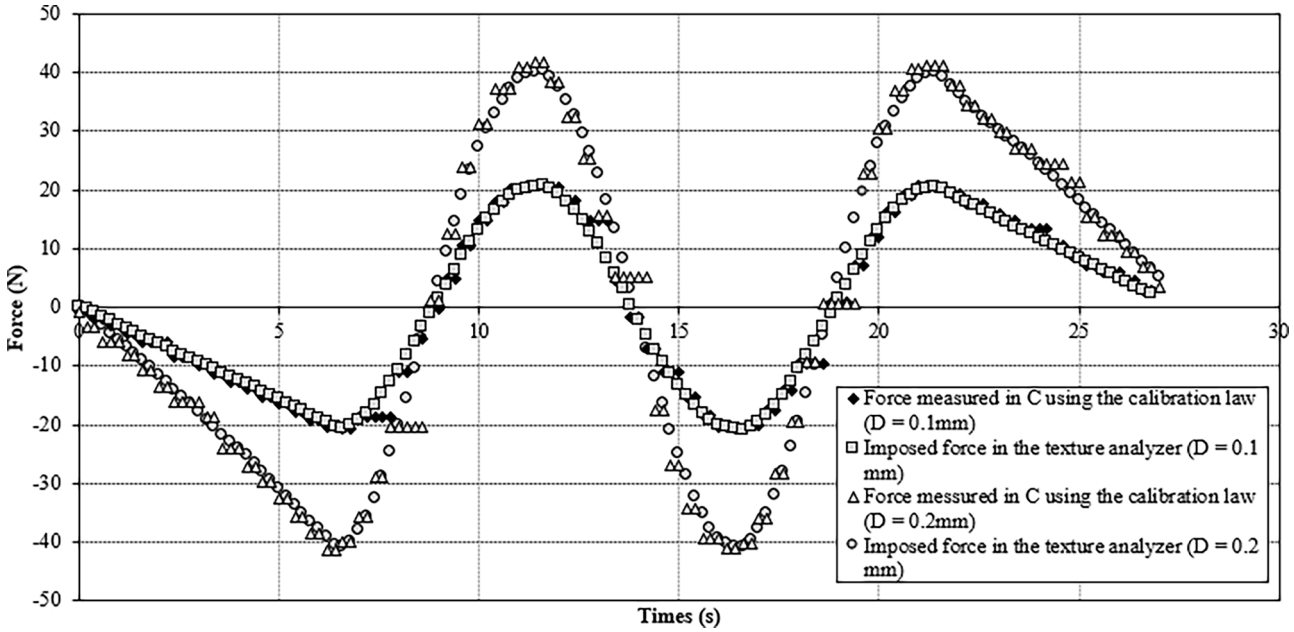

Fig. 8. Temporal evolution of the measured forces at point C applied static laws and on the texture analyzer.

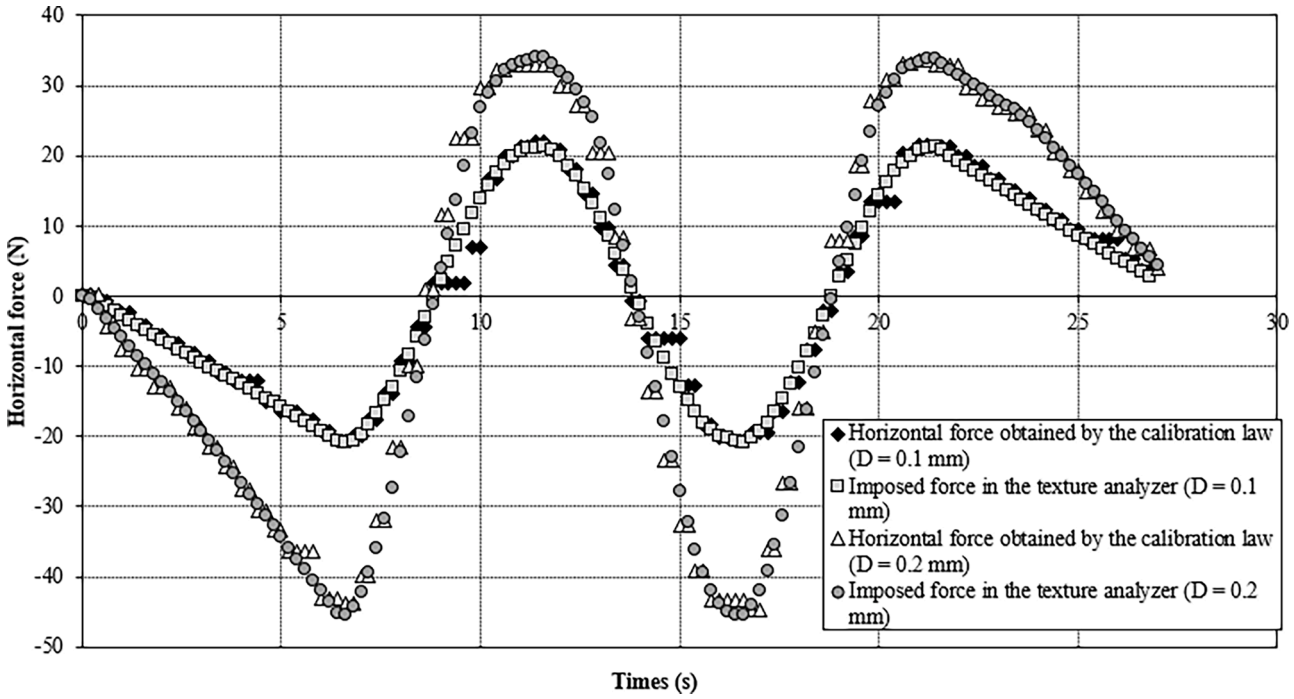

Fig. 9. Temporal evolution of the calculated horizontal forces using the static calibration law and the force delivered by the texture analyzer.

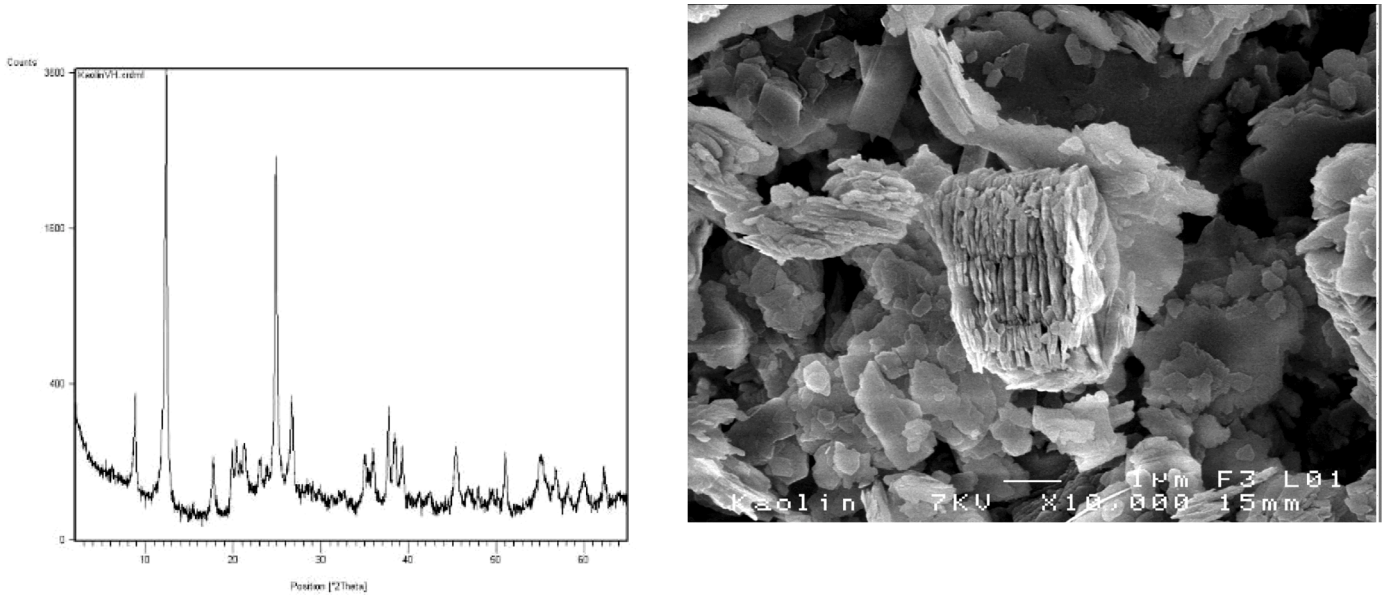

Fig. 10. X-RD pattern of kaolin.

are used to perform the effect of normal stress on the upper surface of the specimen. An arrow in Fig. 12 indicates the upward movement of the plate, leading to the evolution of stresses from position (1) to (3). Position (2) marks the beginning of movement, where the specimen starts to move/slip on the plate. Position (3) of the stress couple characterizes that the specimen is located at the highest position of the plate.

Fig. 12 clearly illustrates the interfacial tribological behavior observed in the experimental program. Initially, during the test, the normal and tangential stresses is located at position (1), illustrating in Fig. 12, corresponding to the lowest point of the specimen. When the plate starts rotating, it causes the specimen to move upward (vertically ascending). This upward movement, combined with the plate rotation, leads to a variation in the normal stress at the Kaolin paste/wall, consequently affecting the tangential stress. These aspects reveal a significant aspect of the friction law elucidated by the friction test. To expand the tribological response and validate the test's reproducibility, the test was replicated with various normal loads.

As shown in Fig. 4b, there was a gap of 0.95 mm between the lower side of the sample holder and the lowest position of the plate. After the tangential stress applied on specimen overcame the static friction stress, the tangential stress initially reduces, and then it increases as the height at the contact point with the specimen rises. As demonstrated in Fig 14, two phenomena can occur during friction testing. When the vertical force is small (less than 150 KPa), a sliding surface appears between the specimen and the steel plate at the contact surface, resulting in an abrasion layer on the surface (Fig. 14a). When the vertical force is large

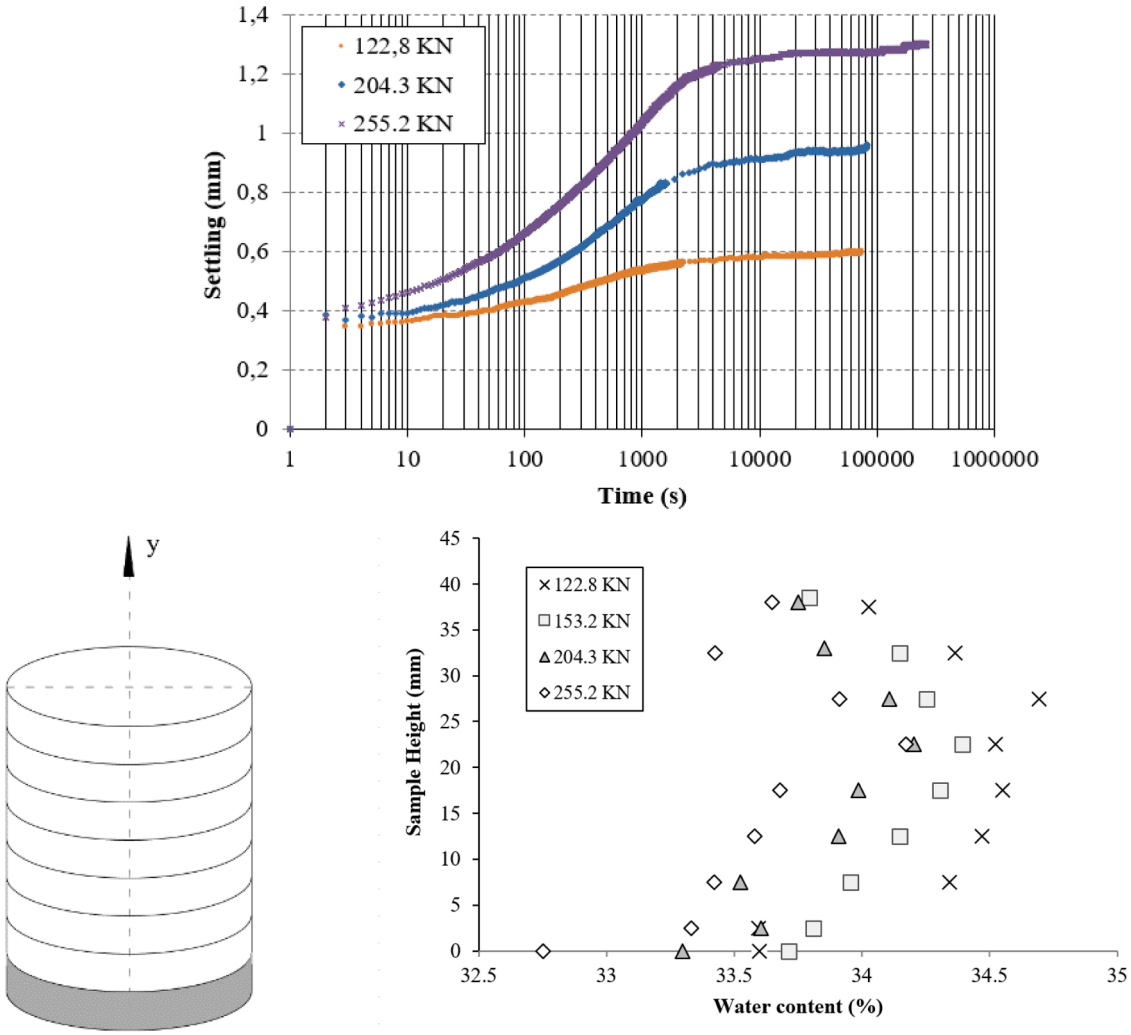

Fig. 11. Water content, w, evolution along specimen height versus the normal load applied on the specimen.

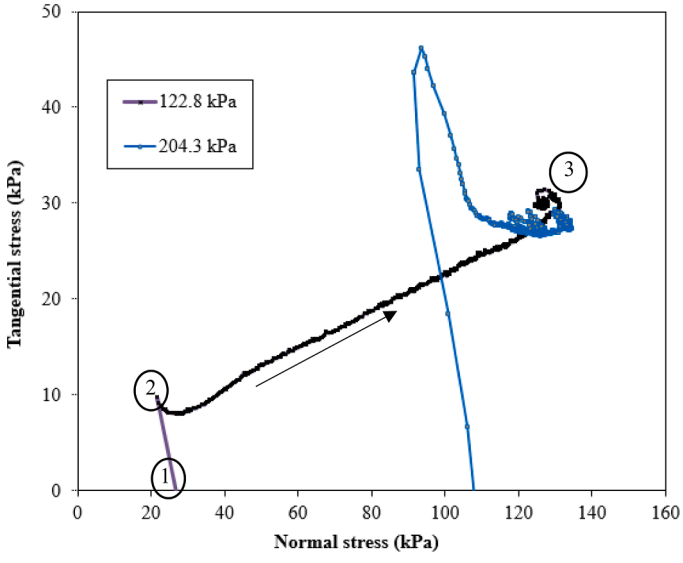

Fig. 12. Illustration of the tangential stress versus the normal stress at the kaolin/smooth wall interface for two tests with $\sigma_{y\ (y=h)}$ values of 122.8 kPa and 204.3 kPa.

(150–250 KPa), a cutting surface appears in a section of the 0.95 mm thick layer, as observed in Fig. 14b. Some materials detach from the specimen during the plate's movement. This residue causes disruption in the shear stress value when the stress exceeds 120 KPa due to changes in the contact surface area compared to the initial contact surface.

From Figs. 12 to 14, the tribological behavior at the interface between kaolin paste/smooth wall is well represented by Mohr-Coulomb behavior. The results presented in Fig. 14 indicate a slight variation in the structuration of the kaolin during the test. When the normal stress exceeds 90 kPa and the shear stress exceeds 25 kPa at the kaolin/wall interface, the recorded data become unstable. The occurrence of a sticked layer during the rotating plate test, as shown in Fig. 13b, can explain instability of recorded data.

4.3. Effect of the friction velocity on tribological characterization of kaolin/smooth wall

The measured values with the normal stress on upper the specimen ranging from 120 to 250 MPa are grouped according to each plate velocity. Fig. 15 shown the effect of the friction velocity on the couple of tangential and normal stress in the interface kaolin paste/smooth wall. Tests are performed with three friction velocities ($V_g = 10^{-3}$, 10^{-2} and 5.10^{-2} m.s^{-1}).

The relationship between tangential stress (τ) and normal stress (σ) can be expressed as follows:

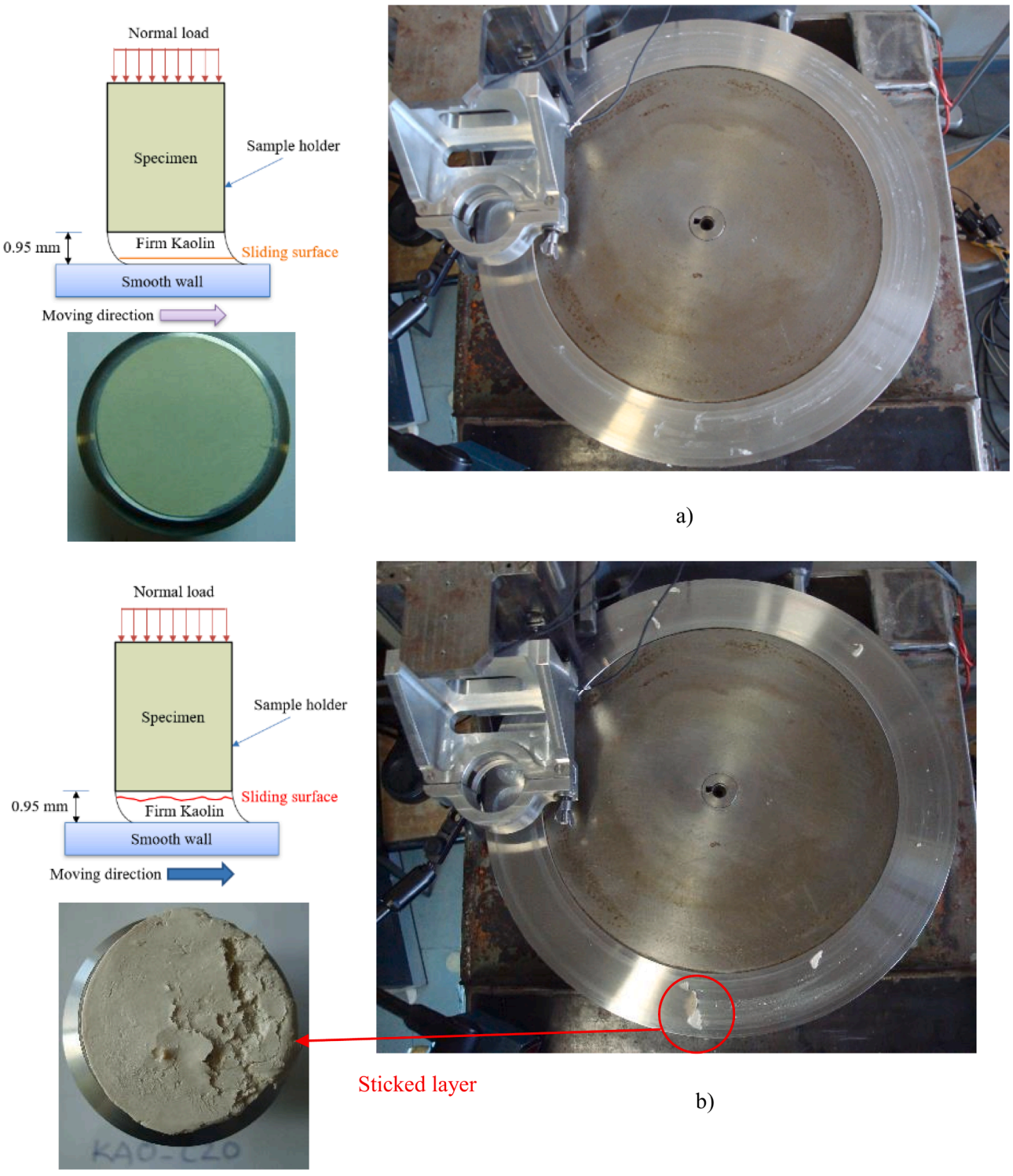

Fig. 13. Two types of sliding surface during testing: (a) test performed with normal stress 122 kPa; (b) test performed normal stress 204 kPa.

$$\tau = C + \mu_d \cdot \sigma \tag{4}$$

where C is a constant, and μ_d is the dynamic friction coefficient.

The results of C and μ_d obtained for smooth wall interface (R_a =0.52 μm) with the friction velocity within a range from $10^{-}3$ m/s to 5.10^{-2} m/s are summarized in Table 1. The value of C can be considered a constant, while μ_d depend on the friction velocity, V_g. The proposed equation describing the tribology of kaolin paste/smooth wall is given by:

$$\mu_d = \mu_{fr} V_g^{n_{fr}} \tag{5}$$

$$\tau = C + \mu_{fr} V_g^{n_{fr}} \cdot \sigma \tag{6}$$

where : μ_{fr} is the apparent friction factor and n_{fr} is index of friction wih μ_{fr} =0.2088 and n_{fr} =0.017 (Fig. 16).

Accepting the hypothesis of a minimal structural evolution potentially induced by the vertical load applied on top of the specimen during the friction testing, the apparent water content of the specimen after

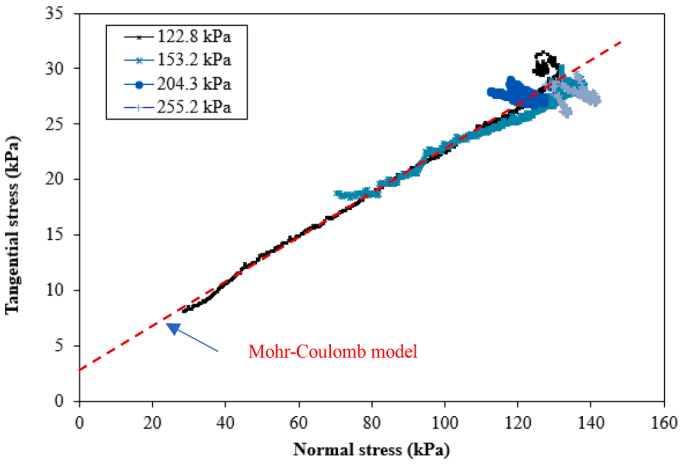

Fig. 14. Dynamic wall friction characterization ($122.8 \leq \sigma_{y\ (y\ =\ h)} \leq 255.2$ kPa).

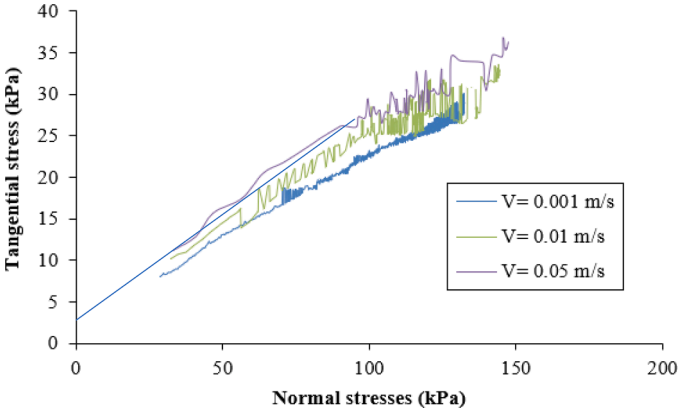

Fig. 15. Evolution of tangential stress versus normal stress at the kaolin paste/smooth wall interface with different friction velocity.

Table 1
Dynamic friction coefficient (μ_d) identification.

Velocity of plate	μ_d (-)	C	R^2 (-)
$Ra = 0.52 - V_g = 10^{-3}$	0.186	3.7	0.98
$Ra = 0.52 - V_g = 10^{-2}$	0.192	3.8	0.95
$Ra = 0.52 - V_g = 5.10^{-2}$	0.199	3.58	0.96

each friction test was determined. The water content was determined in the 5 mm slice of the specimen located near the wall after friction test. The results as shown in Fig. 8 confirm the hypothesis of minimal evolution in the kaolin structure. The results of dynamic friction coefficient are summarized in Table 1. The dynamic friction coefficient decreases with the increasing friction velocity. The results obtained from the experiment are smaller than the values obtained in the research of Perrot et al. (2012). This difference can be explained by the water content of the kaolin mixture, and the plate roughness used in this study is smaller than that in the research of Perrot et al. (2012) and this research not take into account the effect of the normal stresses in the friction dynamic.

5. Conclusions

This study has investigated the tribological behavior at the interface between extrudable kaolin specimens and a smooth metal plate, utilizing the Pion pawn tribometer developed for this purpose. The following findings can be drawn from this research:

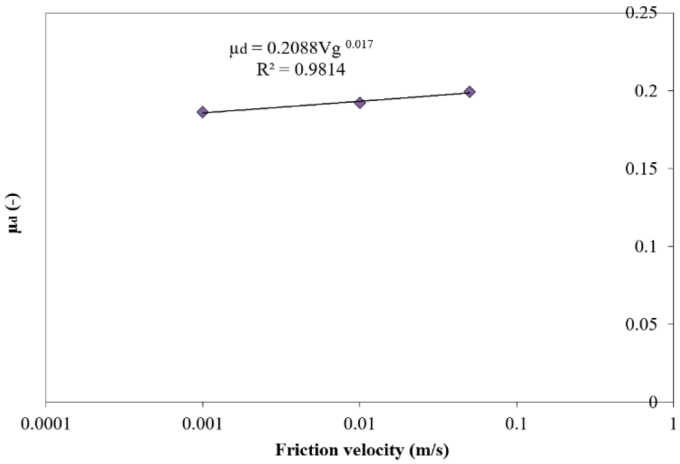

Fig. 16. Proposed relation between the dynamic friction coefficient and the friction velocity.

(1) The Pion pawn tribometer has been developed and calibrated for both static and dynamic modes. This device is designed to investigate the dynamic friction properties of extrudable materials against a rigid wall. Additionally, it can examine the structural changes during the extrusion process by applying increasing force to the mixture over time.
(2) The tribological behavior at the interface between the extrudable kaolin and a smooth wall is effectively characterized by the Mohr-Coulomb model.
(3) Tests conducted with smooth wall ($R_a = 0.52$ μm) demonstrated the effect of the friction velocity within a range from $10^{-}3$ m/s to 5.10^{-2} m/s on the dynamic friction coefficient. The dynamic friction coefficient decreases as the friction velocity increases. A relationship between the dynamic friction coefficient and the friction velocity is proposed for use in modeling the extrusion process.

This test is compatible with firm paste in extrusion process. For future work, the effect of roughness and of mixture water content on the tribological behavior of kaolin and other materials should be experimentally conducted.

CRediT authorship contribution statement

Viet Hai Hoang: Investigation, Visualization, Writing – original draft. **Christophe Lanos:** Conceptualization, Methodology. **Yannick Mélinge:** Conceptualization, Methodology, Visualization.

Declaration of competing interest

The authors declare that they have no known competing financial interests or personal relationships that could have appeared to influence the work reported in this paper.

Data availability

Data will be made available on request.

Acknowledgments

None.

References

Akhoundi, B., Ouzah, R., 2023. Experimental and numerical investigation of rotating bending fatigue of polylactic acid 3D printed parts by an extrusion-based additive manufacturing method. J. Eng. Res. https://doi.org/10.1016/j.jer.2023.07.006.

Akhoundi, B., Sousani, F., 2023. An experimental investigation of screw-based material extrusion 3D printing of metallic parts. J. Eng. Res., 100102 https://doi.org/10.1016/j.jer.2023.100102.

Benbow, J., Bridgewater, J., 1993. Paste Flow and Extrusion. Oxford University Press, UK.

Djelal, C., 2001. Designing and perfecting a tribometer for the study of friction of a concentrated clay-water mixture against a metallic surface. Mater. Struct. 34 (1), 51–58. https://doi.org/10.1007/BF02482200.

Goudjil, N., Vanhove, Y., Djelal-Dantec, C., Kada, H., 2012. Electro-osmosis applied for formwork removal of concrete. J. Adv. Concrete Technol. 10, 301–312. https://doi.org/10.3151/jact.10.301.

Hoang, V.H., 2011, Interaction fluide-structure: comportement tribologique des matériaux minéraux à base cimentaire à l'état frais, Thesis (PhD) in INSA Rennes, France.

Hoang, V.H., Do, T.A., Tran, A.T., Lanos, C., Mélinge, Y., 2023. Effect of electro-osmosis on lubrication of fresh cement paste-based material in contact with a metal wall. Korea Aust. Rheol. J. 35 (3), 157–168. https://doi.org/10.1007/s13367-023-00063-0.

Jayasimha, S.L.N., Lingaraju, K.N., Raju, H.P., 2022. Prediction of surface finish in extrusion honing process by regression analysis and artificial neural networks. Appl. Eng. Sci. 10, 100105. https://doi.org/10.1016/j.apples.2022.100105.

Kandagaddala, R.K., Dhanapal, S.V., Nanthagopalan, P., 2023. Rheological characterization of limestone calcined clay cement pastes with various generations of superplasticizers for pumping applications. J. Build. Eng. 76, 107410. https://doi.org/10.1016/j.jobe.2023.107410.

Kocserha, I., Gömze, L.A., 2010. Friction properties of clay compounds. Appl. Clay Sci. 48 (3), 425–430. https://doi.org/10.1016/j.clay.2010.01.017.

Libessart, L., Djelal, C., de Caro, P., Laiymani, I., 2020. Comparative study of the tribological behaviour of emulsions and demoulding oils at the concrete/formwork interface. Constr. Build. Mater. 239, 117826. https://doi.org/10.1016/j.conbuildmat.2019.117826.

Liddel, P.V., Boger, D.V., 1996. Yield stress measurements with the vane. J. Nonnewton Fluid Mech. 63 (2), 235–261. https://doi.org/10.1016/0377-0257(95)01421-7.

Mélinge, Y., Hoang, V.H., Rangeard, D., Perrot, A., Lanos, C., 2013. Study of tribological behaviour of fresh mortar against a rigid plane wall. Eur. J. Environ. Civ. Eng. 17 (6), 419–429. https://doi.org/10.1080/19648189.2013.786242.

Ngo, T.T., Kadri, E.H., Bennacer, R., Cussigh, F., 2010. Use of tribometer to estimate interface friction and concrete boundary layer composition during the fluid concrete pumping. Constr. Build. Mater. 24 (7), 1253–1261. https://doi.org/10.1016/j.conbuildmat.2009.12.010.

Nguyen, D.H., 2022. Micromechanical approach to determine the effects of surface and interfacial roughness in materials and structure under cosinusoidal normal pressure. Transp. Commun. Sci. J. 73 (1), 31–39. https://doi.org/10.47869/tcsj.73.1.3.

Nguyen, T.T., Do, H.Q., Pham, B.V.A., Nguyen, L.T., 2022. Analysis of perturbes frictional contact problems. Transp. Commun. Sci. J. 73 (1), 61–74. https://doi.org/10.47869/tcsj.73.1.6.

Perrot, A., Lanos, C., Estellé, P., Melinge, Y., 2006. Ram extrusion force for a frictional plastic material: model prediction and application to cement paste. Rheol. Acta 45 (4), 457–467. https://doi.org/10.1007/s00397-005-0074-y.

Perrot, A., Mélinge, Y., Rangeard, D., Micaelli, F., Estellé, P., Lanos, C., 2012. Use of ram extruder as a combined rheo-tribometer to study the behaviour of high yield stress fluids at low strain rate. Rheol. Acta 51 (8), 743–754. https://doi.org/10.1007/s00397-012-0638-6.

Perrot, A., Rangeard, D., Nerella, V.N., Mechtcherine, V., 2019. Extrusion of cement-based materials - an overview. RILEM Tech. Lett. 3 (0), 91–97. https://doi.org/10.21809/rilemtechlett.2018.75.

Spitz, N., Coniglio, N., Libessart, L., El Mansori, M., Djelal, C., 2021. Characterizing tribological behavior of fresh concrete against formwork surfaces. Constr. Build. Mater. 303, 124233. https://doi.org/10.1016/j.conbuildmat.2021.124233.

Tran, A.T., Hoang, V.H., Tran, D.N., Do, T.A., 2022. Effect of adhesion failure and temperature on the mechanical behavior of orthotropic steel bridge deck. Transp. Commun. Sci. J. 73 (1), 52–60. https://doi.org/10.47869/tcsj.73.1.5.

Ulrich, D., Binz, H., 2021. An enhanced design method for 3D contact surfaces on shaft–hub connections joined through lateral extrusion. Appl. Eng. Sci., 100047 https://doi.org/10.1016/j.apples.2021.100047.

Vanhove, Y., Djelal, C., 2021. Influence of the formwork removal by polarization on the facing aesthetics in reinforced concrete. Constr. Build. Mater. 284, 122841. https://doi.org/10.1016/j.conbuildmat.2021.122841.

Vignes, J., Schmidt, F., Dusserre, G., Dalmasso, J.F., 2013. Effect of moisture on the behaviour of an extruded clay paste. Key Eng. Mater. 2230–2236, 554–557. https://doi.org/10.4028/www.scientific.net/KEM.554-557.2230.

Xia, Y., Yang, K., Feng, X., Wang, Y., 2022. Tribological properties of modified kaolin doped polymer as polytetrafluoroethylene grease additive. Tribol. Int. 173, 107612. https://doi.org/10.1016/j.triboint.2022.107612.